

## The Madden–Julian Oscillation’s Influence on African Easterly Waves and Downstream Tropical Cyclogenesis

MICHAEL J. VENTRICE, CHRIS D. THORNCROFT, AND PAUL E. ROUNDY

*Department of Atmospheric and Environmental Science, University at Albany, State University of New York, Albany, New York*

(Manuscript received 1 November 2010, in final form 21 March 2011)

### ABSTRACT

The influence of the Madden–Julian oscillation (MJO) over tropical Africa and Atlantic is explored during the Northern Hemisphere summer months. The MJO is assessed by using real-time multivariate MJO (RMM) indices. These indices divide the active convective signal of the MJO into 8 phases. Convection associated with the MJO is enhanced over tropical Africa during RMM phases 8, 1, and 2. Convection becomes suppressed over tropical Africa during the subsequent RMM phases (phases 3–7). African convective signals are associated with westward-propagating equatorial Rossby waves.

The MJO modulates African easterly wave (AEW) activity. AEW activity is locally enhanced during RMM phases 1–3 and suppressed during RMM phases 6–8. Enhanced AEW activity occurs during periods of enhanced convection over tropical Africa, consistent with stronger or more frequent triggering of AEWs as well as more growth associated with latent heat release. Enhanced AEW activity occurs during the low-level westerly wind phase of the MJO, which increases the cyclonic shear on the equatorward side of the AEW, increasing its instability.

Atlantic tropical cyclogenesis frequency varies coherently with the MJO. RMM phases 1–3 show the greatest frequency of tropical cyclogenesis events whereas phases 7 and 8 show the least. RMM phase 2 is also the most likely phase to be associated with a train of three or more tropical cyclones over the tropical Atlantic. This observed evolution of tropical cyclogenesis frequency varies coherently with variations in AEW activity and the large-scale environment.

---

### 1. Introduction

The Madden–Julian oscillation (MJO) is the leading mode of intraseasonal rainfall variability in the tropics (Madden and Julian 1972; Zhang 2005). While often perceived to be less important over West Africa, the MJO has recently received more attention in the West African monsoon region (WAM; e.g., Sultan et al. 2003; Matthews 2004; Lavender and Matthews 2009) during boreal summer. Most previous work has focused on the mechanisms that affect rainfall variability in this region. This paper considers how the MJO modulates the intraseasonal variability of African easterly wave (AEW) activity over Africa and tropical cyclogenesis activity over the main development region (MDR; 5°–25°N, 15°–60°W).

The WAM is modulated by interactions across different spatial and temporal scales over West Africa and the eastern Atlantic basin. Janicot and Sultan (2001) and Sultan et al. (2003) identified two dominant frequency bands for the intraseasonal variability in WAM convection: one in the 10–25-day range (with a peak around 15 days) and one in the 25–60-day range (with a peak around 30 days). Mounier and Janicot (2004) suggest that the activity in the 10–25-day range results from a fluctuation in zonal advection of moisture between the Atlantic and the Sahel, which they associate with a quasi-biweekly zonal dipole (Mounier et al. 2008). The longer time-scale variability (25–60-day band) is thought to be associated with the MJO (Pohl et al. 2009).

Over Africa, the fluctuations associated with the MJO are less well documented than for other tropical regions and our understanding of these events remains incomplete. Several studies have suggested that the influence of the MJO on sub-Saharan Africa is weak (e.g., Knutson and Weickmann 1987; Annamalai and Slingo 2001; Wheeler

---

*Corresponding author address:* Michael Ventrice, University at Albany, State University of New York, 1400 Washington Ave., Albany, NY 12222.  
E-mail: mv945965@albany.edu

and Weickmann 2001; Roundy and Frank 2004) and others suggest there is no influence at all (e.g., Knutson et al. 1986; Murakami et al. 1986). These conclusions are sensitive to the variables analyzed, as well as the choice of diagnostic for the MJO. In marked contrast, Matthews (2004) suggested that the MJO can exert substantial influence on the WAM. He found that when convection is suppressed over the Indian Ocean warm pool region in association with the MJO, an atmospheric equatorial Kelvin wave propagates from the Indian Ocean along the equator toward the east and an equatorial Rossby wave (ERW) propagates toward the west. These two waves meet roughly 20 days later over West Africa and are associated with negative midtropospheric temperature anomalies that favor deep convection. This interaction of equatorial waves is timed with the strongest convectively active signal of the MJO over tropical Africa (RMM phase 1). The ERW associated with the MJO has also been demonstrated by Roundy and Frank (2004), and is also suggested in Wang and Rui (1990). Maloney and Shaman (2008) confirmed the influence of the MJO on intraseasonal variability over Africa using Tropical Rainfall Measuring Mission (TRMM) rainfall estimates. They concluded that the MJO explains up to 30% of the 30–90-day variance of the rainfall in the WAM. Pohl et al. (2009) established that this MJO-related signal over Africa is mainly characterized by westward propagation at the Sahel latitudes, consistent with convectively coupled ERWs.

Given that WAM rainfall varies in association with the MJO, we should expect that AEW activity varies on similar time scales. Leroux et al. (2010) showed that AEW activity in the West African region varies on temporal scales consistent with the MJO. They also showed that periods of enhanced AEW activity were preceded by periods of enhanced convection in the entrance region of the AEJ consistent with the triggering hypothesis for the origin of AEWs (see Thorncroft et al. 2008). They also observed an intensification of the upstream half of the AEJ prior to the enhancement of AEW activity, highlighting the role of the basic state in determining AEW variability in addition to variability in triggering. Although Leroux et al. (2010) did not emphasize the MJO, it seems likely that it would contribute to this intraseasonal variability. This work complements theirs by focusing more directly on the possible modulation of AEW activity by the MJO.

The known relationship between the WAM and tropical cyclones (e.g., Landsea et al. 1998; Hopsch et al. 2007, 2010) suggests the need to investigate whether the MJO-related variability in the WAM impacts downstream tropical cyclone activity. For example, it is possible that periods of enhanced AEW activity are associated with

periods of enhanced tropical cyclone activity given the more frequent and/or intense AEWs. In addition to AEW activity, we suspect the influence of the MJO on the WAM could also result in variations of the downstream environment over the tropical Atlantic, which might impact the probability of the formation of tropical cyclones [e.g., vertical shear; Aiyyer and Thorncroft (2010)].

In addition to the indirect effects through the modulation of the WAM, it is also important to consider the direct impacts the MJO may have on the probability of tropical cyclogenesis. Frank and Roundy (2006) proposed that tropical cyclogenesis within roughly  $20^\circ$  of the equator might be modulated by the family of zonally propagating equatorial and near-equatorial waves, and the MJO. They, along with others (e.g., Maloney and Hartmann 2000; Mo 2000; Maloney and Shaman 2008; Klotzbach 2010), suggest that the MJO can influence tropical cyclogenesis by increasing upward vertical motion and convection (which also tends to lead to increased deep-layer moisture) and/or by increasing the low-level vorticity and altering the local vertical shear pattern. Modulation of Atlantic tropical cyclones by the MJO has been previously examined by Maloney and Hartmann (2000) and Mo (2000). Maloney and Hartmann (2000) show that Gulf of Mexico and western Caribbean hurricanes were 4 times more likely to occur when the MJO projects lower-tropospheric westerly wind anomalies over the eastern Pacific rather than when the MJO projects lower-tropospheric easterly wind anomalies. Mo (2000) found a significant modulation of tropical cyclone activity by the MJO west of  $60^\circ\text{W}$ , where tropical cyclone activity varied with the first principal component (PC) of Eastern Hemisphere OLR used to diagnose the MJO. This paper analyzes the MJO in a similar approach to Klotzbach (2010) by using the Wheeler and Hendon (2004) real-time multivariate MJO (RMM) indices. Klotzbach (2010) found statistically significant differences between RMM phases 1 and 2 in contrast to phases 6 and 7 with respect to sea level pressure, zonal wind, and relative humidity over the tropical Atlantic. During RMM phases 1 and 2, as a MJO event forms over the western Indian Ocean and the convective signal begins to move northeastward, the MDR experiences lower pressures, reduced vertical wind shear, and enhanced midlevel humidity, all of which tend to favor enhanced tropical cyclone formation and intensification. Klotzbach (2010) concludes that 85% of storms that formed in the MDR during phases 1 and 2 reached hurricane strength, while only 45% of storms forming in phases 6 and 7 reached hurricane strength.

In this paper, we examine the association of each RMM phase with weather variability over Africa and the downstream tropical Atlantic. Our work answers the

following two questions: How does AEW activity over Africa and the tropical Atlantic Ocean evolve with the MJO? How is the MJO associated with the frequency and distribution of tropical cyclogenesis events over the tropical Atlantic Ocean? This paper is structured as follows. Section 2 discusses the datasets and methodology. Section 3 shows how the basic state over Africa and the tropical Atlantic evolves with the phase of the MJO and examines the association between the MJO and AEW activity. In section 4, we discuss how the MJO modulates tropical cyclone formation over the tropical Atlantic Ocean, emphasizing the role of AEWs. Section 5 discusses our results and conclusions.

## 2. Data and methodology

We investigate the MJO only during the Northern Hemisphere summer months (June–October, JJASO). To identify the phase of the MJO, we use the Wheeler and Hendon (2004) RMM indices. The indices are the PC time series of the two leading empirical orthogonal functions (EOFs) of combined daily mean tropical (averaged 15°N–15°S) 850- and 250-hPa zonal wind and OLR anomalies. The seasonal cycle and a portion of the low-frequency variability associated with El Niño–Southern Oscillation (ENSO) are removed before calculating the EOF. Two indices, RMM1 and RMM2, were constructed to observe MJO events independent of seasonality constraints. RMM1 and RMM2 are approximately in quadrature and describe the average large-scale, eastward-propagating convective and circulation anomalies associated with the MJO. The evolution of the MJO is visualized in a two-dimensional phase–space diagram, with RMM1 as the horizontal and RMM2 as the vertical Cartesian axes. The RMM indices are expressed as a selection of eight phases with each phase corresponding to a rough geographical location of the active convective phase of the MJO. RMM phase 1 consists of convection associated with the MJO over the western equatorial Indian Ocean, whereas RMM phase 8 represents the eastward propagation of the MJO signal over the Western Hemisphere.

We calculated composite patterns by averaging fields of data over each one of the eight RMM phases during JJASO (for 1989–2008). Data were averaged over the set of all dates for a particular phase when amplitudes were greater than one standard deviation. Anomalies for all composited fields were constructed as differences from the seasonal cycle. The seasonal cycles for all fields were constructed by using the annual cycle and its first four harmonics. Statistical significance testing was performed on all anomalies by bootstrap random resampling tests. These tests were applied by constructing a

number of samples equal in size to the anomaly dataset, which is obtained by randomly drawing a new set of anomalies with replacement from the original dataset and binning the anomalies for each randomly drawn set. One thousand iterations were used for each test. We chose the year range to be consistent with the European Centre for Medium-Range Weather Forecasts (ECMWF) Interim Re-Analysis described below. We subjectively identified 42 MJO events by using the RMM indices. For clarification, the average time spent in each RMM phase is about 4–8 days.

Consistent with many previous studies, the convective signal of the MJO is highlighted by using the National Oceanic and Atmospheric Administration's (NOAA) daily averaged interpolated OLR dataset at 2.5° horizontal resolution from 1989 to 2008 (Liebmann and Smith 1996). Variations in the large-scale environment and AEW activity are explored by using the ECMWF-Interim dataset at 1.5° horizontal resolution. ECMWF-Interim is a reanalysis product that incorporates both observations and model data and is the latest product from ECMWF covering the years since 1989. This ECMWF product has been shown to be a significant improvement over previous ECMWF reanalysis products (Simmons et al. 2007). ECMWF-Interim wind data were used to calculate low-level vorticity and shear. Total column water vapor (TCWV) data were used from the dataset to estimate atmospheric moisture.

To provide a large-scale perspective of the MJO and to illustrate the methodology that will be used throughout this paper, we show here a composite of the MJO evolution based on the RMM indices (Fig. 1). Figure 1 highlights the eastward propagation of the MJO's convective signal along the equator using OLR anomalies. During RMM phase 1, active convection is located across the Western Hemisphere, over parts of Africa, and over the western equatorial Indian Ocean (Fig. 1a). Convective anomalies then increase in geographical extent and amplitude over the Indian basin and move northward and eastward. The associated convective anomalies enhance the Indian monsoon during phases 2–5 (Figs. 1a–e). In phase 5, the mean convective anomaly signal latitudinally shrinks and moves at a faster phase speed through the mean position of the intertropical convective zone (ITCZ). This pattern continues into phase 8 when the MJO is associated with enhanced convection over the eastern Pacific and tropical Africa.

Following Leroux et al. (2010), AEW activity was diagnosed by calculating the eddy kinetic energy (EKE) based on wind data that were filtered in a 2–10-day band ( $u'$  and  $v'$ ). The EKE, defined as

$$\text{EKE} = \frac{1}{2}(u'^2 + v'^2), \quad (1)$$

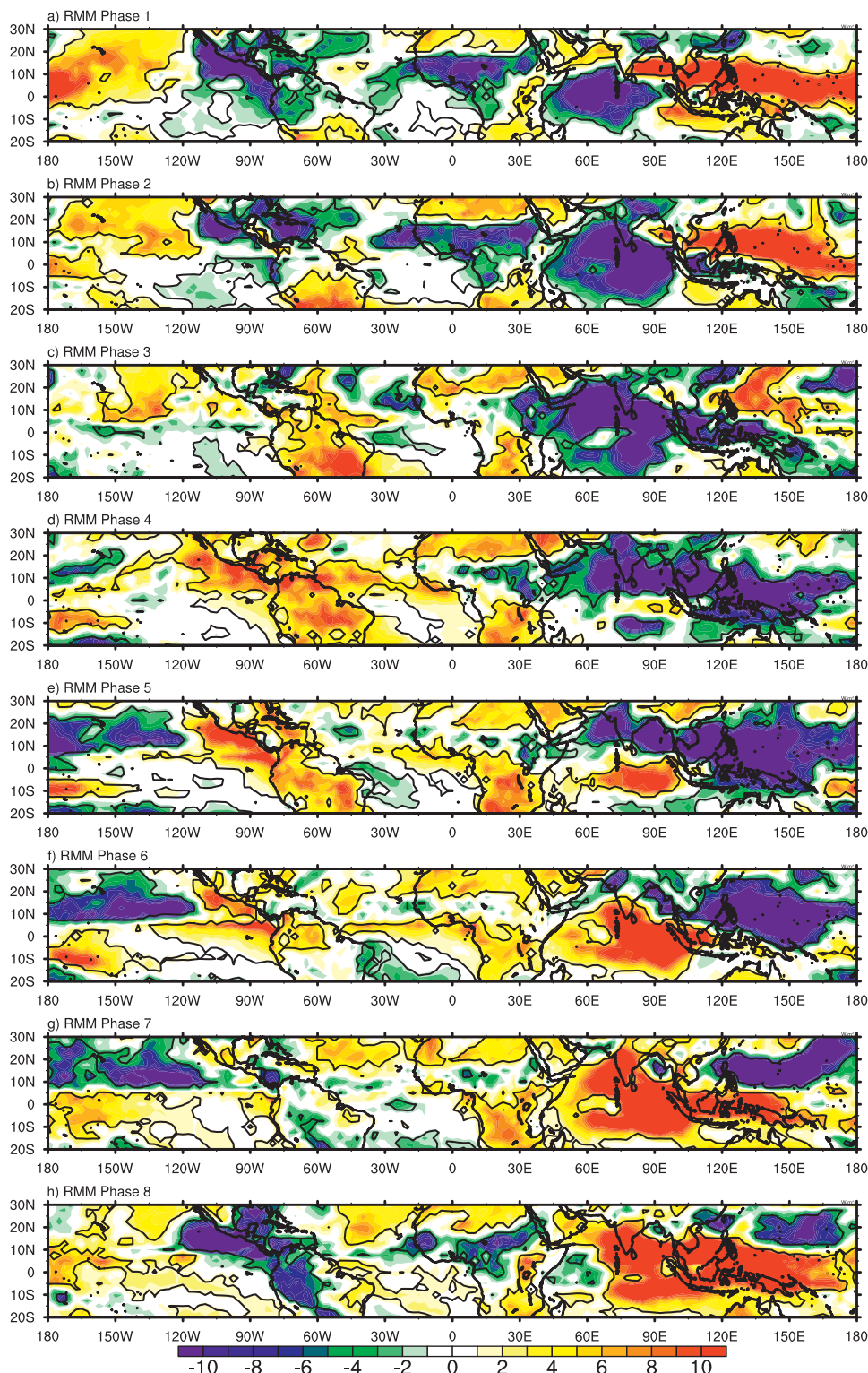


FIG. 1. NOAA daily averaged interpolated OLR anomalies for the Northern Hemisphere summer months (JJASO) from 1989 to 2008 for each RMM phase. Anomalies statistically significantly different than zero at the 95% level are within the solid black contour. Shaded units are in  $W m^{-2}$ ; the shading interval is  $1 W m^{-2}$ .

was based on the ECMWF-Interim data and was calculated at 700 hPa for each RMM phase during the same time period.

To help interpret some aspects of the MJO signal over West Africa and the tropical Atlantic, we will consider the role played by ERWs following the work of Matthews (2004) and Janicot et al. (2010). Convection associated with convectively coupled ERWs is explored using the NOAA daily averaged interpolated OLR dataset. Wavenumber–frequency filtering for ERWs was applied on the OLR anomalies following the methodology of Kiladis et al. (2009). The ERW filter includes wavenumbers 1–10 westward and periods ranging from 10 to 48 days with the maximum frequency along the ERW dispersion curve at 90-m equivalent depth.

An analysis of tropical cyclogenesis events was performed by binning the number of tropical cyclones that formed during each RMM phase (from 1974 to 2009, excluding 1978). We define a genesis event as a tropical cyclone that was at least classified as a tropical depression in the National Climatic Data Center's International Best Track Archive for Climate Stewardship (IBTrACS) dataset (Knapp et al. 2010). We analyzed tropical cyclone development in a region similar to that of Maloney and Shaman (2008), concentrating on the eastern Atlantic ITCZ region between 60°W and the African coast. This area received relatively little emphasis in the investigations of Mo (2000) and Maloney and Hartmann (2000), but it is a region that we expect to be strongly impacted by AEW variability (cf. Hopsch et al. 2010).

### 3. The influence of the MJO on the intraseasonal variability of convection over Africa

#### a. OLR

To investigate the evolution of convection over Africa, we focus on the composited OLR signal over the Atlantic basin and Africa (recall Fig. 1). The MJO convective signal first appears over the western Atlantic basin in phase 7 (Fig. 1g). During this time, the convection in the position of the mean ITCZ is enhanced over the western Caribbean and regions of the tropical western Atlantic. During RMM phase 8 (Fig. 1h), negative OLR anomalies first appear over Africa and persist into phase 2 (Fig. 1b). The strongest convective signal over tropical Africa occurs in phase 1 (Fig. 1a), a time when convection associated with the MJO signal begins to form over the equatorial Indian Ocean (Fig. 1a). These negative OLR anomalies extend farther to the west over Africa during phase 2 (Fig. 1b) and can be seen over the eastern tropical Atlantic during phase 3. This westward-moving

convective signal is discussed further below. A reduction of negative OLR anomalies is observed locally over western-central tropical Africa during phase 3 (Fig. 1c). Phases 8, 1, and 2 clearly represent the convectively active phase of the MJO over tropical North Africa. This convective signature over Africa shown in RMM phases 1 and 2 has a similar structure to the first EOF of the June–September 10–200-day filtered OLR shown in Fig. 1 of Lavender and Matthews (2009) [see also Fig. 1 in Janicot et al. (2009) and Fig. 1a in Mounier et al. (2008)]. This suggests that the MJO is the dominant contributor to variability in convection on 10–200-day time scales.

RMM phase 3 occurs when the strongest MJO convective signal is located over the eastern Indian Ocean warm pool. In the Western Hemisphere, a transition from negative to positive OLR anomalies is evident over western-central tropical Africa (Fig. 1c). These positive OLR anomalies strengthen in magnitude over the Guinea coast during RMM phase 4 and persist through phase 7. Phases 3–7 represent the convectively suppressed phase of the MJO over western-central tropical Africa. We acknowledge a difference in convective structures over Africa when using the RMM indices with respect to Lavender and Matthews's (2009) principal component (PC) warm pool analysis (see their Fig. 6). The RMM indices are associated with a richer pattern of evolution for convection over tropical Africa, which likely arises because they include circulation information in addition to OLR information. Further, the two RMM PCs combined explain more of the total variance in the MJO than the single PC of Lavender and Matthews. Lavender and Matthews's PCs are based solely on OLR, and therefore may miss some of the critical dynamics of the MJO signal, which can alter the convective signature over tropical Africa.

Several authors have discussed the westward-moving convective signature that characterizes the MJO influence over tropical North Africa between RMM phases 1 and 3 (e.g., Wang and Rui 1990; Matthews 2004; Roundy and Frank 2004; Janicot et al. 2009; Lavender and Matthews 2009; Pohl et al. 2009). Janicot et al. (2010) suggest that the westward movement of convection is associated with ERWs. To explore this possibility, we filter OLR in the wavenumber–frequency domain for ERWs, and then average the result according to the RMM phase. Figure 2 shows the results superimposed on composite unfiltered OLR anomalies. We note that the top panel in this figure is RMM phase 4 (Fig. 2a). This result confirms that some of the enhanced convection over Africa during RMM phases 8, 1, and 2 is associated with the westward-moving convectively active ERW signal. Also, some of the suppressed convection over Africa during RMM phases 5–7 is associated with

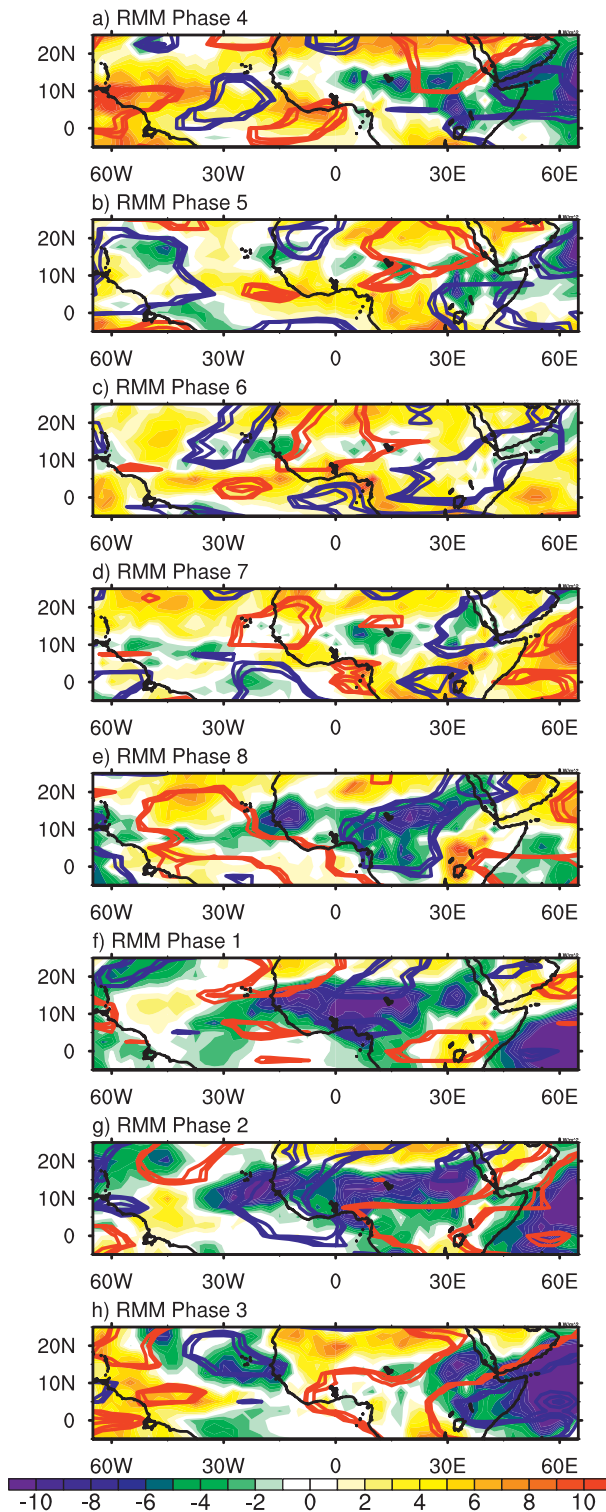


FIG. 2. As in Fig. 1, but the ERW space-time-filtered OLR anomalies are composited and contoured (red) if they are negative (positive). ERW-filtered OLR anomalies are contoured if they are statistically different than zero at the 95% level. Shaded units are in  $W m^{-2}$ ; the shading interval is  $1 W m^{-2}$ .

a convectively suppressed ERW signal. For brevity, we will only discuss the composited convectively active ERW signal; however, do note that the composited convectively suppressed ERW signal during RMM phases 5–7 acts to locally suppress convection over Africa during these times.

The convectively active signal associated with the ERW can be tracked over the eastern Indian Ocean and southern Asia, where convection is locally suppressed by the MJO at the same time. The composited convectively active ERW is south of the Arabian Peninsula during phase 6 (Fig. 2c) and begins to move over tropical Africa during phase 7 (Fig. 2d). Areas of negative OLR anomalies can be seen collocated with the convectively active phase of the ERW during these times. During phase 8, convection is first enhanced with the ERW over the Darfur Mountains ( $\sim 30^{\circ}E$ ) (Fig. 2e). The ERW signal then moves over interior tropical Africa, resulting in a large intensification of convection during phase 1 (Fig. 2f). The ERW signal is located over the coast of tropical West Africa in phase 2, enhancing convection over and downstream of the Guinea Highlands region. Between phases 2 and 3, the ERW signal shifts northwestward and is later located over the tropical Atlantic during phases 3 and 4 (Figs. 2h and 2a, respectively). We speculate that the ERW may help to trigger AEWs over the topography of Africa, which would amplify the convective signal over tropical Africa during these times. This result suggests ERWs substantially modulate rainfall associated with the WAM on subseasonal temporal scales in association with the convectively active MJO signal over Africa.

Convection over Africa may influence the generation of AEWs. Mekonnen et al. (2006) found that the Darfur Mountains are a preferential area for the formation of AEWs. Kiladis et al. (2006) showed that convection in the Darfur region precedes AEWs over West Africa. AEWs form during periods favorable for deep convection, or enhanced convective triggering over Africa (e.g., Thorncroft et al. 2008). ERWs may influence such convective events. We hypothesize that when convection associated with the ERW signal is favored over the Darfur Mountains, a period of enhanced AEW activity follows. We will explore this concept in the following section.

*b. Impacts of the MJO on AEW activity*

Figure 3 shows 700-hPa EKE anomalies for each RMM phases. The EKE anomalies vary coherently through the different phases of the MJO, suggesting that the MJO modulates AEW activity. Phases 1–3 have large prominent regions of enhanced EKE with longitudinal extents greater than  $30^{\circ}$ . Positive EKE anomalies occur during phase 1 over interior tropical Africa (Fig. 3a). These

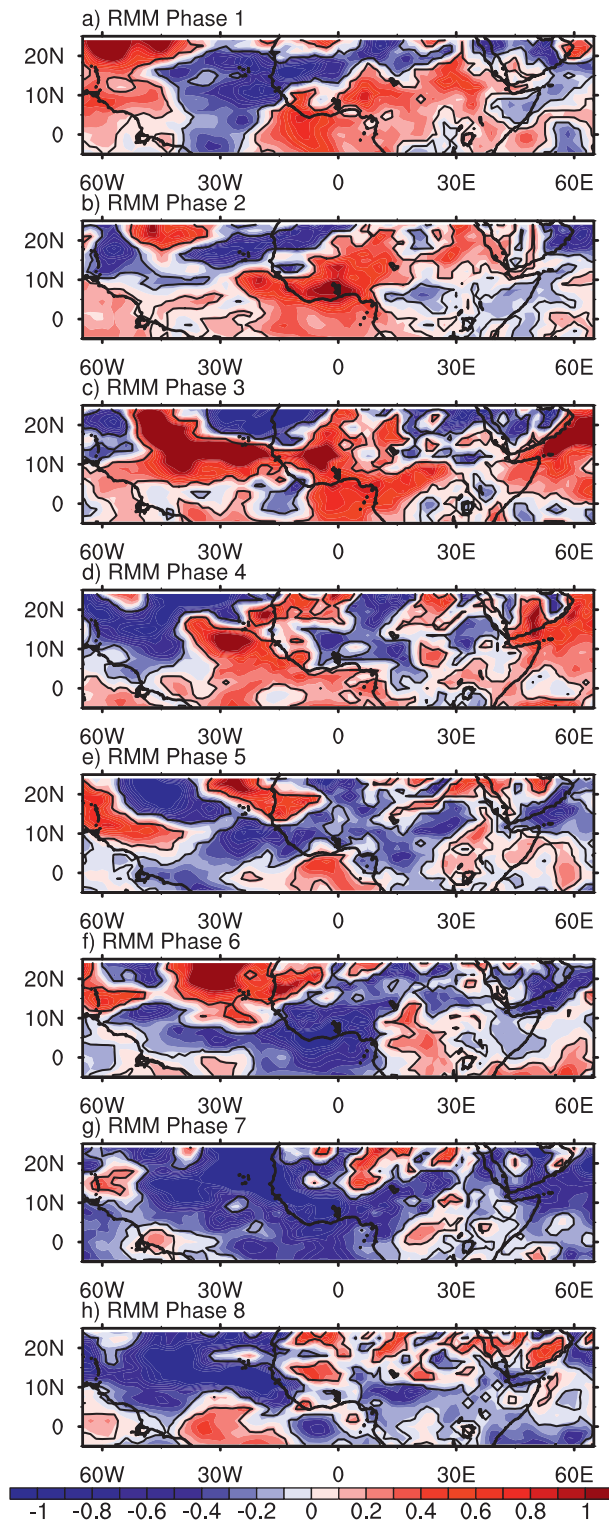


FIG. 3. The 2–10-day-filtered EKE anomalies at 700 hPa for each RMM phase. Anomalies statistically significantly different than zero at the 95% level are within the solid black contour. Shaded units are in  $\text{m}^2 \text{s}^{-2}$ ; the shading interval is  $0.1 \text{ m}^2 \text{s}^{-2}$ .

positive EKE anomalies increase in magnitude and extend slightly to the west during phase 2 (Fig. 3b). During this phase, the strongest positive anomalies are located over sub-Saharan Africa. During phase 3, the strongest positive EKE anomalies shift poleward and extend farther west over western tropical Africa (Fig. 3c). By RMM phase 4, the strongest positive EKE anomalies are located over the eastern tropical Atlantic (Fig. 3d). Over eastern and central Africa, the positive EKE anomalies switch to negative anomalies, representing a reduction of AEW activity. This transition from positive to negative EKE anomalies continues through RMM phase 5, highlighting an increase in negative EKE anomalies over tropical Africa (Fig. 3e). Phases 6 and 7 have the most prominent regions of negative EKE anomalies over tropical Africa. Phase 8 consists of significant negative EKE anomalies over the coast of West Africa extending westward over the MDR. A westward shift of negative EKE anomalies during RMM phases 6–8 is observed over tropical West Africa. It is interesting to note how these patterns compare to the two EOFs of EKE seen by Leroux et al. (2010). Their EOF1 is characterized by single-signed anomalies over West Africa and the tropical Atlantic somewhat similar to what we observe in Fig. 3. This provides further evidence that the variability explored by Leroux et al. (2010) was likely dominated by the MJO.

The westward movement of positive EKE anomalies during RMM phases 1–4 lags the westward-propagating negative OLR anomalies shown in Fig. 1 by one RMM phase. Negative EKE anomalies occur together with the first convectively active phase of the MJO over West Africa (RMM phase 8). Positive EKE anomalies over tropical Africa develop one phase later (RMM phase 1). These positive EKE anomalies remain over West Africa through RMM phase 3. Convection first becomes more locally suppressed over Africa during RMM phase 3 yet positive EKE anomalies remain over West Africa. The EKE anomalies then swap to negative anomalies over tropical Africa one RMM phase later (RMM phase 4).

We expect AEW activity to be enhanced by two mechanisms: (i) more intense convection, which provides increased convective triggers and/or latent heat release for AEW growth (see Thorncroft et al. 2008), and (ii) a more unstable AEJ (Leroux and Hall 2009). We have discussed that convective triggers lead periods of enhanced AEW activity in the previous paragraph. Leroux et al. (2010) also found a strong lead–lag asymmetry between convection and AEW activity. The convective signal was strongest 2–5 days prior to a period of enhanced AEW activity. This result is similar to ours, in that enhanced convection leads enhanced AEW activity by one RMM phase. Leroux et al. (2010) also observed

a westward-moving OLR signal, a result that they suggest may arise from intraseasonal wave modes that have Rossby wave structures or the westward propagation of clusters of AEWs (and which was observed here; see Fig. 2). Furthermore, Leroux et al. (2010) explore the AEJ in relation to AEW activity and emphasized an acceleration of the AEJ entrance region prior to a period of enhanced AEW activity. This acceleration of the AEJ was explained to be influenced by a large stretch of anomalous easterly winds that slowly propagated northward over India on intraseasonal time scales. We now explore the MJO–AEJ relationship using the RMM indices below.

*c. Impacts of the MJO on the AEJ*

To explore the variation of the AEJ between the different RMM phases, we consider the zonal wind at 700 hPa (Fig. 4). The analysis of Fig. 4 is complex; therefore, we will first focus on the evolution of the dynamical signal of the MJO in the 700-hPa wind field. The influence of the MJO on the 700-hPa zonal wind flow over Africa reflects the low-level (850 hPa) dynamical structure of the MJO.

During the initiation of an MJO event (phase 1), significant westerly wind anomalies are observed equatorward of the AEJ core over West Africa and the eastern tropical Atlantic (Fig. 4a). These anomalous equatorward westerly winds are associated with the beginning stage of the low-level westerly wind phase of the MJO. Westerly wind anomalies extend westward and amplify in magnitude over the eastern Pacific (not shown). The anomalous easterly winds observed east of 15°E extend over the Indian Ocean and grow in magnitude (not shown). These easterly wind anomalies are associated with the tail end of the low-level easterly wind phase of the MJO. Therefore, over Africa during RMM phase 1, a transition from anomalous low-level equatorial easterly winds to low-level equatorial westerly winds occurs.

As convection over the Indian Ocean grows northward and eastward during RMM phase 2, the anomalous equatorial westerly winds shift eastward and grow in magnitude over equatorial Africa, consistent with the eastward progression of the MJO (Fig. 4b). These anomalous equatorial westerly winds continue to grow in magnitude and shift eastward during RMM phases 3 and 4 (Figs. 4c and 4d, respectively). Anomalous easterly wind anomalies form over the eastern tropical Atlantic during RMM phase 5 (Fig. 4e). These anomalous winds are associated with the beginning stage of the low-level equatorial easterly wind phase of the MJO. Easterly wind anomalies extend westward and amplify over the eastern Pacific (not shown). The equatorial easterly wind anomalies grow in magnitude and extend eastward through RMM phase 8, consistent with the eastward

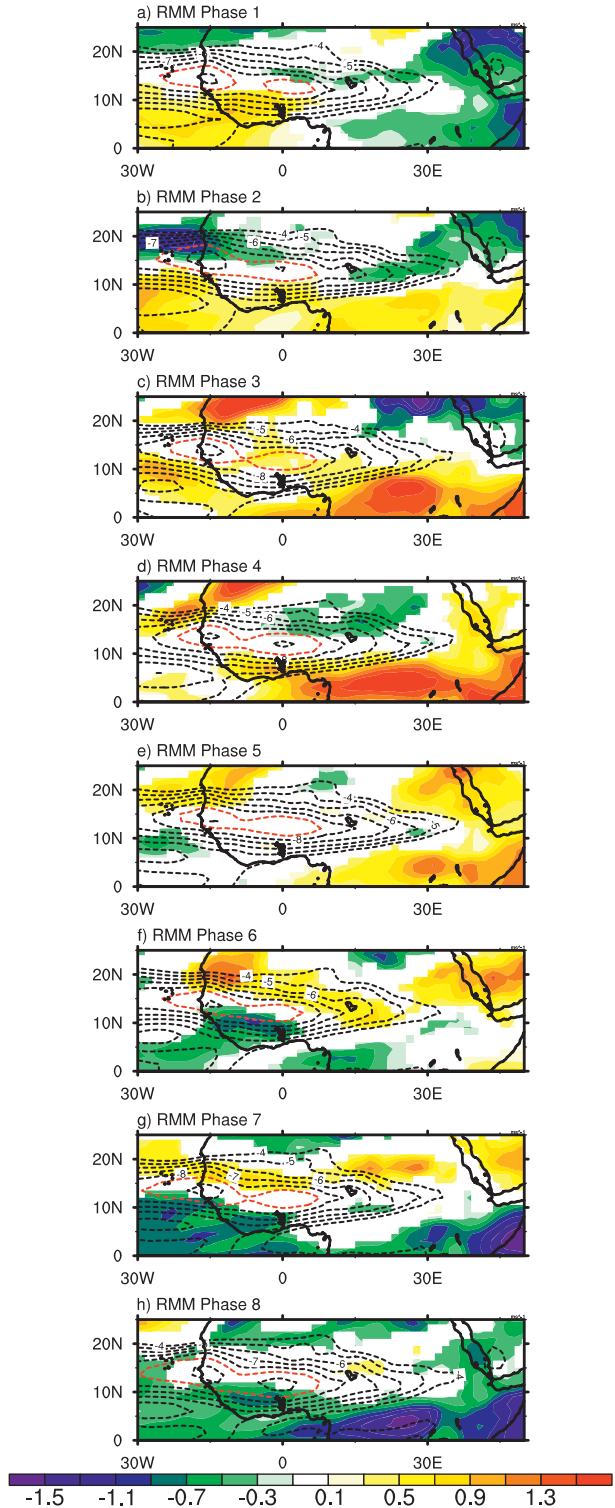


FIG. 4. The 700-hPa zonal wind anomalies for each RMM phase. Anomalies statistically significant different than zero at the 95% level are shaded. Shaded units are in  $\text{m s}^{-1}$ ; the shading interval is  $0.2 \text{ m s}^{-1}$ . Total raw easterly zonal wind is composited for each RMM phase and contoured. Contour units are in  $\text{m s}^{-1}$ , the contour range is from  $-10$  to  $-4 \text{ m s}^{-1}$ , and the contour interval is  $1 \text{ m s}^{-1}$ . Negative contours are dashed. Red-dashed contour highlights the  $-9 \text{ m s}^{-1}$  contour.

progression of the MJO (Figs. 4f–h). In summary, a coherent eastward-progressing equatorial wind pattern is expressed, such that anomalous equatorial westerly winds occur over the eastern tropical Atlantic during RMM phases 1–4, followed by anomalous equatorial easterly winds during RMM phases 5–8.

We now focus on the structure of the AEJ during each RMM phase. The modulation of the AEJ involves two contributions. The first being the low-level equatorial wind structure of the MJO. This equatorial wind pattern will act to influence the horizontal shear of the jet on the equatorward side. The other contributor is local convection associated with the MJO over Africa. Anomalous convection equatorward of the jet generates potential vorticity near the level of the jet, which would act to strengthen the jet following the argument of Thorncroft and Blackburn (1999). Further, anomalous convection north or south of the AEJ would act to latitudinally shift the jet. Keeping these principles in mind, we begin our analysis when convection associated with the MJO is first observed over Africa during RMM phase 8.

During RMM phase 8, a zonally oriented strip of enhanced convection over Africa is observed along roughly 13°N (recall Fig. 1h). An equatorward acceleration of the AEJ core is observed, which is also suggestive of a southward-shifted AEJ (Fig. 4h). This acceleration of the AEJ is highlighted by the large area of  $-9 \text{ m s}^{-1}$  winds over West Africa with the largest area of  $-10 \text{ m s}^{-1}$  winds centered over 0° when compared to all other RMM phases. Therefore, the AEJ core is strongest during this RMM phase (8) and is shifted to the south. However, the equatorial easterly wind phase of the MJO, which has the greatest expression over Africa during RMM phase 8, causes a reduction in the gradient of zonal wind. This suggests the AEJ is less unstable, which is consistent with low AEW activity (recall Figs. 3f–h). In support of this, the sign reversal in absolute vorticity is less negative than any other RMM phase (not shown). Therefore, even though phase 8 is associated with a stronger AEJ, which is generally expected to be more unstable, the impact of the low-level dynamical structure of the MJO supersedes this.

During RMM phases 1 and 2, enhanced convection is observed north of 15°N (recall Figs. 1a and 1b). Easterly wind anomalies are observed poleward of the AEJ core during these phases, indicating a northward shift of the AEJ, especially over the coast of West Africa during RMM phase 2. Easterly wind anomalies are also observed over the AEJ entrance region during these periods, highlighting an eastward extension of the AEJ during RMM phase 2. To provide perspective, the  $-8 \text{ m s}^{-1}$  wind contour extends to 18°E, roughly 5° farther east than for any other RMM phase. This

eastward extension of the AEJ occurs when a large stretch of easterly wind anomalies lift northward from the Indian Ocean to over India, consistent with the observations of Leroux et al. (2010) (not shown). Equatorial westerly winds associated with the MJO form over Africa during RMM phase 1 and expand eastward during phase 2. This causes a tightening of the zonal wind gradient, and indicates a more unstable jet, which is expected to enhance AEW growth. Further, the sign reversal in absolute vorticity becomes more negative during RMM phase 1, and most negative during phase 2, indicating the jet is indeed more unstable at these times (not shown).

Following the eastward extension of the AEJ, a reduction in convection occurs over tropical West Africa during RMM phase 3 (recall Fig. 1c). This is consistent with significant westerly wind anomalies over the AEJ core during this time. During the following RMM phase 4, significant westerly wind anomalies over the eastern tropical Atlantic are observed poleward of the AEJ, consistent with an equatorward shift of the jet. Significant westerly wind anomalies extend eastward and remain poleward of the AEJ core throughout RMM phase 7, indicating the AEJ is located farther south during these RMM phases in contrast to RMM phases 1 and 2.

In summary, consistent with the convectively active phases of the MJO, the AEJ is enhanced during RMM phases 8, 1, and 2. The jet is strongest during RMM phase 8; however, it is less unstable and is located farther south than RMM phases 1 and 2. This RMM phase is consistent with anomalously low AEW activity over tropical Africa and especially over the MDR. The AEJ becomes more unstable during RMM phase 1 and most unstable during RMM phase 2. This enhancement of jet instability is related to the low-level equatorial westerly wind phase of the MJO over Africa during this time. Also during RMM phases 1 and 2, the AEJ is observed to shift northward when AEW activity is anomalously high. Furthermore, during RMM phase 2, the AEJ extends farthest poleward over the coast of West Africa and farthest eastward over central Africa than during any other RMM phase. This longitudinal extension of the AEJ is hypothesized to play a significant role in AEW development (see Leroux et al. 2010).

We have explored the relationship of the subseasonal variability of AEW activity based on the RMM phases. The results suggest that the subseasonal variability of AEW activity arises due to the MJO directly influencing convective triggers over tropical Africa, as well as AEJ characteristics. Our results are similar to those of Leroux et al. (2010) and confirm that most of their results are related to the MJO. Our results are consistent with the analysis of Leroux et al. (2010) and is represented by

RMM phase 2, which can range on average from 4 to 8 days. Further, in contrast to Leroux et al. (2010), we find that an acceleration of the AEJ entrance occurs after, and during, a period of anomalously high AEW activity. We now explore the extent to which the variability in AEW activity has an influence on downstream tropical cyclone activity.

**4. Tropical cyclogenesis analysis**

Given that most Atlantic tropical cyclones form in association with AEWs over the tropical Atlantic, we expect that the variability in AEW activity, highlighted in the previous section, will impact tropical cyclogenesis frequency. To evaluate this, we now explore and interpret the extent to which there is a coherent relationship between the RMM indices and tropical cyclogenesis inside the MDR. We define the MDR as the area between 5°–25°N and 15°–60°W. This analysis extends previous work on the same topic (e.g., Maloney and Shaman 2008; Klotzbach 2010) since in addition to considering variations in the large-scale environment, we emphasize here the role of the AEW variability on tropical cyclogenesis over the MDR. We suggest that the MJO might modulate tropical cyclone activity via “weather-related impacts” through variability in AEWs (e.g., Hopsch et al. 2010) and an “environmental impact” through variability in large-scale parameters known to impact the probability of tropical cyclogenesis such as vertical shear and moisture (e.g., Roundy and Frank 2004; Aiyyer and Thorncroft 2010; Klotzbach 2010). We perform a simple count of the number of tropical cyclones that formed during each phase of the MJO to highlight which RMM phases favor tropical cyclone development (Fig. 5a). Confidence intervals for the total number of tropical cyclones for each RMM phase are assessed by bootstrap random resampling tests.

The distribution of tropical cyclogenesis events inside the MDR for each RMM phase when amplitudes are greater than  $1\sigma$  is shown in Fig. 5a. The result shows that tropical cyclone development inside the MDR occurs most during RMM phases 1, 2, and 5. The peak of the tropical cyclone events in these RMM phases is statistically significantly different from the counts in RMM phases 7 and 8 at the 95% level. These results are somewhat consistent with those of Klotzbach (2010), who found RMM phases 1 and 2 were the most favorable RMM phases for tropical cyclone activity over the entire Atlantic basin. He found when averaging RMM phases 1 and 2 that large-scale atmospheric conditions were more favorable for developing tropical cyclones (e.g., reduced vertical wind shear and higher atmospheric moisture).

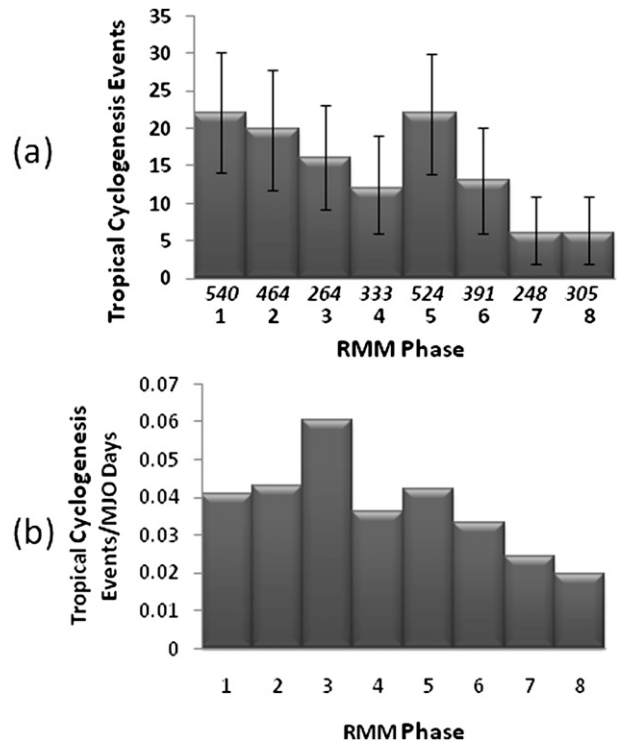


FIG. 5. (a) Tropical cyclogenesis JJASO climatology (1974–2009) for each RMM phase for tropical cyclones formed only within the MDR. The number of MJO days for each composite is placed above each RMM phase number. Error bars indicate the 95% confidence interval. (b) As in (a), but normalized by the number of MJO days for each RMM phase.

However, he did not consider other individual RMM phases in his analysis.

A gradual downward trend of tropical cyclogenesis events occurs during RMM phases 1–4. Intriguingly, a second peak in tropical cyclogenesis events is revealed during RMM phase 5 with a more rapid decline in tropical cyclogenesis events during RMM phases 6–8. To assess if the tropical cyclogenesis counts are real and not manifested due to the varying number of dates that compose each composite, we divide the number of tropical cyclogenesis events by the number of MJO days (greater than  $1\sigma$ ) for each RMM phase (Fig. 5b). The results reveal that during RMM phases 1, 2, and 5 a tropical cyclone is twice as likely to spawn inside the MDR when compared to RMM phase 8. However, during RMM phase 3, a tropical cyclone is 3 times more likely to spawn inside the MDR when compared to RMM phase 8. Therefore, the peaks in RMM phases 1, 2, and 5 are largely reduced due to the number of sampling days. An analysis of the large-scale environmental conditions is further needed to interpret the tropical cyclogenesis variability within the RMM indices, which is provided below.

### a. Large-scale environmental conditions

To relate the tropical cyclone peaks to the well-known favorable parameters of tropical cyclogenesis, we first show 200–925-hPa vertical wind shear anomalies of the zonal wind over the MDR (Fig. 6). We interpret the reduction in vertical wind shear over the MDR by the location of strongest convection associated with the MJO.

During RMM phases 1–4, enhanced convection associated with the MJO progresses eastward and northward over the Indian Ocean. Downstream (to the east) of the deep convection over the Indian Ocean, anomalous upper-level easterly winds form due to convective outflow. This anomalous upper-level convective outflow acts to reduce the vertical wind shear over the MDR. This reduction in vertical wind shear is illustrated by anomalous easterly shear over the MDR at this time (Figs. 6a–d). The opposite is true for RMM phases 5–8, containing significant westerly shear anomalies, or an enhancement in vertical wind shear over the MDR (Figs. 6e–h). The enhancement of vertical wind shear occurs when deep convection associated with the MJO is located over the eastern Pacific. This convective feature consists of dynamics similar to those found during an El Niño, and produces upper-level westerly convective outflow over the MDR. These conditions are consistent with an enhancement of vertical wind shear over the MDR. Therefore, the MJO modulates the vertical wind shear over the MDR on intraseasonal time scales. A significant reduction in vertical wind shear over the MDR is observed during RMM phases 1–4, with a significant enhancement during RMM phases 5–8. The enhancement of vertical wind shear during RMM phase 8 occurs during a time when convection is enhanced over tropical Africa. This suggests the modulation of the vertical wind shear over the MDR is driven largely by the location of the deepest convection associated with the MJO, and not by local convection over Africa (cf. Aiyer and Thorncroft 2010).

Next, total column water vapor (TCWV) anomalies are shown in Fig. 7 for each RMM phase. Significant positive TCWV anomalies, or an anomalously moist troposphere, develop over the MDR during RMM phase 1 (Fig. 7a). Positive TCWV anomalies over the MDR become more positive during phase 2 and most positive in phase 3 (Figs. 7b and 7c). Positive TCWV anomalies during RMM phases 1–3 are all roughly north of 10°N over the MDR, highlighting a moist atmosphere over the MDR. A transition from positive to negative TCWV anomalies occurs during RMM phases 4 and 5. Significant negative TCWV anomalies then form over the MDR during RMM phase 6, become most negative in phase 7, and remain negative through phase 8 (Figs. 7f–h).

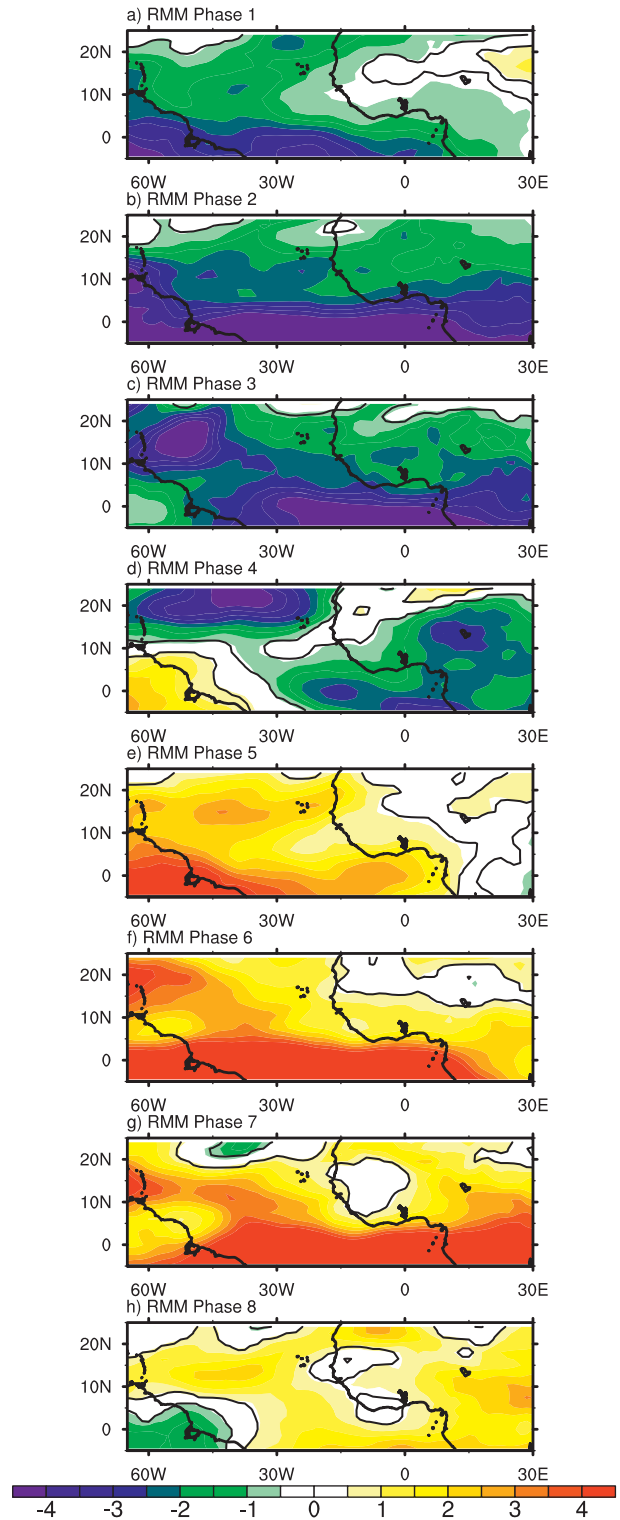


FIG. 6. The 200–925-hPa zonal vertical wind shear anomalies for each RMM phase. Anomalies statistically significantly different than zero at the 95% level are shaded. Shaded units are in  $\text{m s}^{-1}$ ; the shading interval is  $0.5 \text{ m s}^{-1}$ .

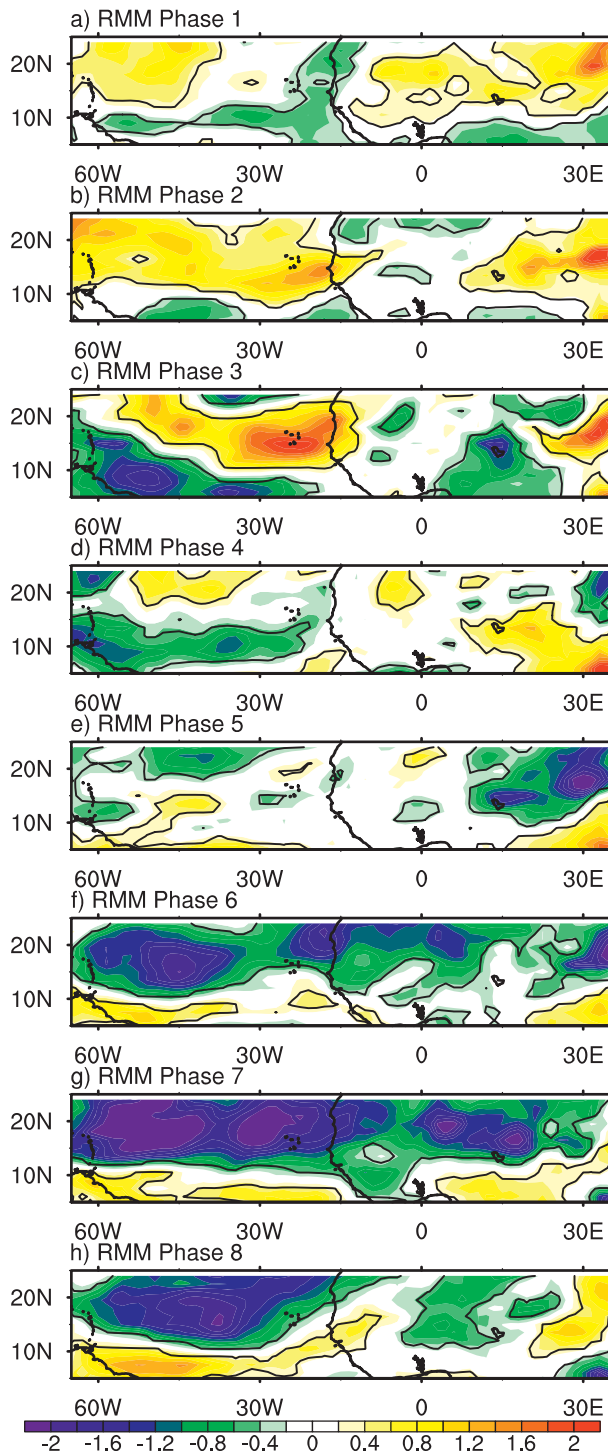


FIG. 7. TCWV anomalies for each RMM phase. Anomalies statistically significantly different than zero at the 95% level are shaded. Shaded units are in mm; the shading interval is 0.02 mm.

Positive TCWV anomalies during RMM phases 5–8 are observed mostly south of 10°N, possibly hinting at a southward shift of the Atlantic ITCZ. Recall that a southward shift of the AEJ also occurs during these RMM phases (Figs. 4e–h).

Finally, low-level (925 hPa) relative vorticity is plotted in Fig. 8 for each RMM phase. The low-level relative vorticity field is modulated by two contributions. The first being the low-level wind structure of the MJO and the second being the location and intensity of the local convection. During RMM phases 1–4, large regions of enhanced relative vorticity are observed over the MDR. This pattern is consistent with the low-level westerly wind phase of the MJO, collocated with enhanced convection over the MDR. During RMM phase 1, scattered regions of significant positive relative vorticity anomalies are observed over the north-central MDR (Fig. 8a). Negative relative vorticity anomalies are found equatorward of this region. This pattern is more coherent during RMM phase 2, with stronger positive anomalies over the entire MDR (Fig. 8b). During RMM phase 3, the positive relative vorticity anomalies are oriented in a narrow-latitudinal band, which seems to recurve northward over the MDR (Fig. 8c). We hypothesize this recurvature of low-level relative vorticity is diabatically generated from enhanced convection over the MDR, which follows a similar pattern in nature (recall Fig. 1c). A narrow band of positive relative vorticity anomalies is later observed over the north-central MDR during RMM phase 4 (Fig. 8d).

During the subsequent RMM phases 5–8, the low-level easterly wind phase of the MJO is located over the MDR. These phases are consistent with large areas of suppressed convection over the MDR. Therefore, mostly negative relative vorticity anomalies are observed over this region (Figs. 8e–h). Therefore, the low-level vorticity field over the MDR varies coherently between the different RMM phases. This result is consistent with the low-level dynamical signal of the MJO and in situ convection over the MDR.

*b. Discussion of MDR tropical cyclogenesis*

Klotzbach (2010) found RMM phases 1 and 2 to contain the highest frequency of tropical cyclogenesis over the Atlantic. He also found that these phases contained statistically significant differences (compared to RMM phases 6 and 7) in the large-scale environment, in reference to significant reductions in vertical wind shear, anomalously high moisture, and enhanced low-level cyclonic relative vorticity. Our results are consistent with the observations of Klotzbach (2010); however, in addition we find enhanced tropical cyclogenesis activity during RMM phase 3. Furthermore, we find that RMM

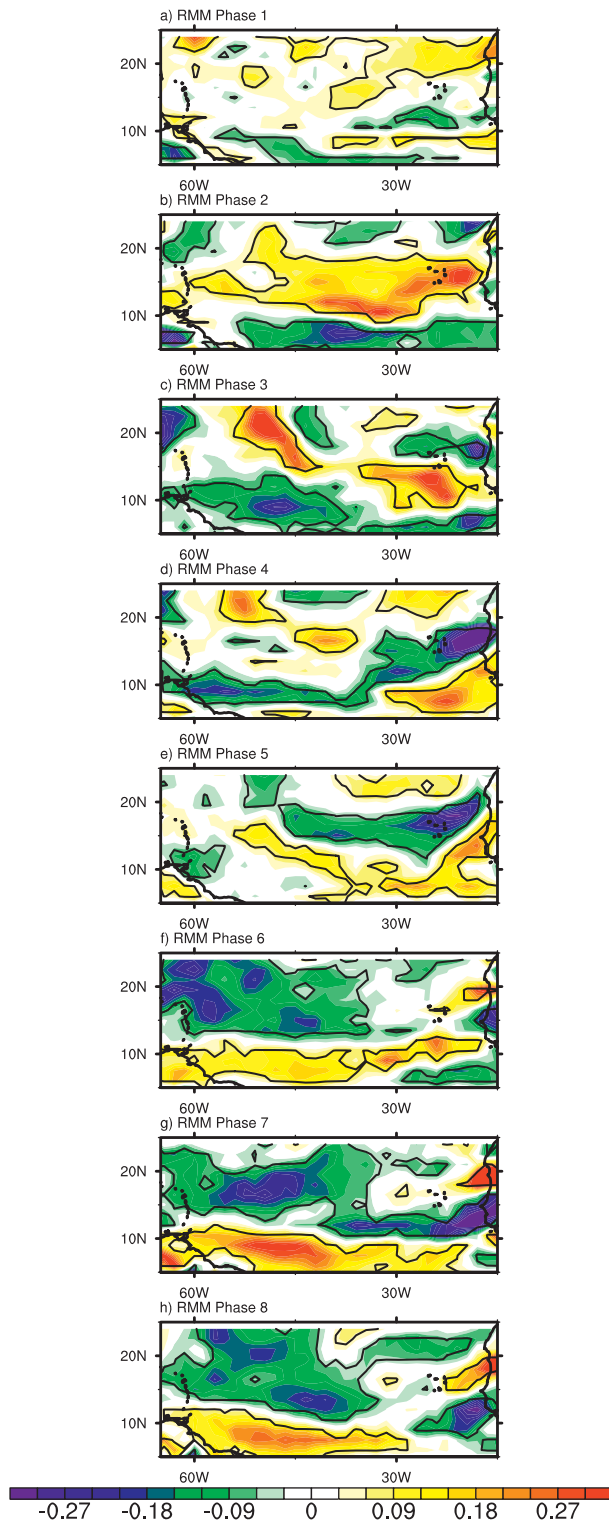


FIG. 8. The 925-hPa relative vorticity anomalies for each RMM phase. Anomalies statistically significantly different than zero at the 95% level are shaded. Shaded units are in  $10^{-5} \text{ s}^{-1}$ ; the shading interval is  $0.03 \times 10^{-5} \text{ s}^{-1}$ .

phases 1–3 are associated with a period of anomalously high AEW activity (recall Figs. 3a–c). Therefore, this period of enhanced tropical cyclone activity in the MDR entails a period of enhanced AEW activity, or more frequent–stronger seedlings. Therefore, we are confident that these phases truly favor MDR tropical cyclogenesis and are not manifested due to the large number of sampling days.

We hypothesize that the suppressed tropical cyclone activity during phases 7 and 8 results in part from reduced AEW activity over tropical West Africa and the eastern tropical Atlantic. AEWs that are either less frequent and/or weaker might reduce the frequency of tropical cyclogenesis. Furthermore, over the MDR, these phases contain enhanced vertical wind shear, significant areas of negative low-level vorticity anomalies, and very dry atmospheric conditions, all of which are unfavorable conditions for tropical cyclogenesis.

The distribution of tropical cyclogenesis events during RMM phases 1–3 and 7 and 8 evolves together with AEW activity over Africa. When EKE values are anomalously high over both West Africa and the MDR (RMM phases 1–3), tropical cyclogenesis events are high inside the MDR. The opposite is true during RMM phases 7 and 8. This relationship highlights the potential influence of the MJO on upstream AEW activity and the development of tropical cyclones inside the MDR.

### c. *Trains of tropical cyclones*

Due to the chaotic nature of tropical cyclogenesis, tropical cyclones generally form randomly where conditions are most favorable. However, occasionally, multiple tropical cyclones develop over the MDR in association with a consecutive set of easterly waves. We call these sequences of tropical cyclones a train. For this to occur, large-scale environmental conditions must be favorable for an extended period of time. Furthermore, during these periods of favorable large-scale environmental conditions, AEW activity must also be high for an extended period of time. The MJO is one possible phenomenon that can create such periods. Trains of tropical cyclones are not documented in the literature and so the processes that create them remain to be explored. We define a “tropical cyclone train” as a group of three or more named tropical cyclones that occur with at most 4 days between genesis dates. We use a four-date threshold due to the 3–5-day periodicity of AEWs. Following this methodology, we identified 20 tropical cyclone trains forming between  $0^{\circ}$ – $25^{\circ}$ N and  $15^{\circ}$ – $60^{\circ}$ W from 1974 to 2009 during August–September. To provide perspective, Fig. 9 shows the 1974–2009 (August–September) grouping climatology of the number of tropical cyclones that occur in different sequences within

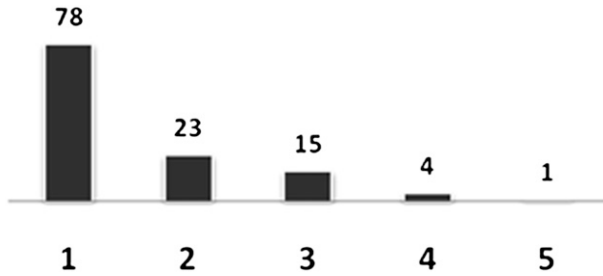


FIG. 9. An August–September climatology (1974 to 2009) of tropical cyclogenesis groups occurring within the 0°–25°N band. The columns represent the total number, or group, of tropical cyclones that contain tropical cyclogenesis events occurring within at most 4 days apart.

the 0°–25°N band and at most 4 days between genesis dates. Column 1 consists of all tropical cyclogenesis events occurring with no other tropical cyclogenesis events within a 4-day range on either side of the genesis date. Column 2 consists of all sequences containing two tropical cyclogenesis events occurring within at most 4 days. The remaining columns (3–5) consist of all sequences of tropical cyclogenesis events that pertain to our definition of a tropical cyclone train. No single tropical cyclone is counted twice in the climatology. Therefore, tropical cyclone trains consist of only 17% of the total grouping climatology.

To isolate tropical cyclone trains developing in association with a coherent MJO signal, we identify trains that occur with an MJO event with an amplitude greater than  $1\sigma$ . There are now 14 tropical cyclone trains remaining out of the climatology (Fig. 10). This result shows that 14 out of the 20 tropical cyclone trains occurred when the RMM amplitude was greater than  $1\sigma$ . This ratio suggests that when a tropical cyclone train occurs, it commonly occurs during a strong MJO event. We investigate if tropical cyclone trains occur during preferable phases of the MJO below.

By individually separating the tropical cyclones into their appropriate RMM phase spaces, we find that the most favorable phase for a train to occur is in phase 2 (statistically significantly different from the counts of all other RMM phases at the 95% level), which is also a statistically significant favorable phase for tropical cyclone development (Fig. 11). We show the total number of tropical cyclones in trains for each RMM phase, rather than the actual number of trains for each RMM phase due to the problem of observing a train that occurs during RMM phase swaps. This result is consistent after decreasing the RMM amplitude threshold to  $0.5\sigma$ ; however, there are more counts in RMM phases 1 and 3 (not shown).

Figure 12 shows the distribution of normalized tropical cyclone train day values for each RMM phase. A

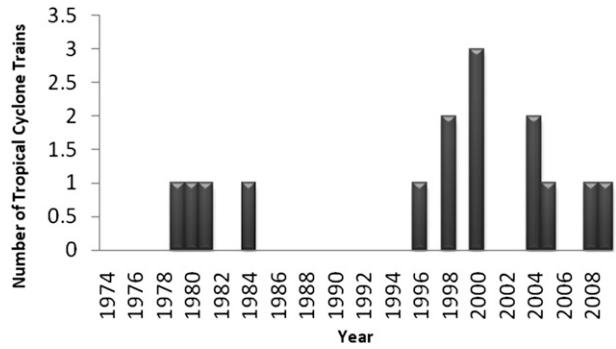


FIG. 10. An August–September climatology (from 1974 to 2009) of tropical cyclone trains from 0° to 25°N, only using dates with an MJO event with an amplitude greater than  $1\sigma$ .

separate category is added, summing all dates when a tropical cyclone train occurred when there was no coherent MJO signal (amplitude  $<1\sigma$ ). Tropical cyclone days were normalized for each RMM phase by the amount of MJO days with an amplitude greater than  $1\sigma$  for each phase. We normalized the tropical cyclone days occurring with no coherent MJO signal by the amount of MJO days with an amplitude less than  $1\sigma$  for all RMM phases. The result shows that the normalized tropical cyclone day value of 23% in RMM phase 2 is more than twice as large as the normalized tropical cyclone train day value when there is no coherent MJO signal (10%). This result is statistically significant at the 90% level.

Over the MDR, RMM phase 2 contains the largest geographical area of statistically significant positive low-level relative vorticity and TCWV anomalies, with a significant reduction in zonal vertical wind shear (recall Figs. 6b, 7b, and 8b). Further, RMM phase 2 is convectively active with anomalously high AEW activity over Africa. Hence, the tropical cyclones that compose the tropical cyclone train climatology are most

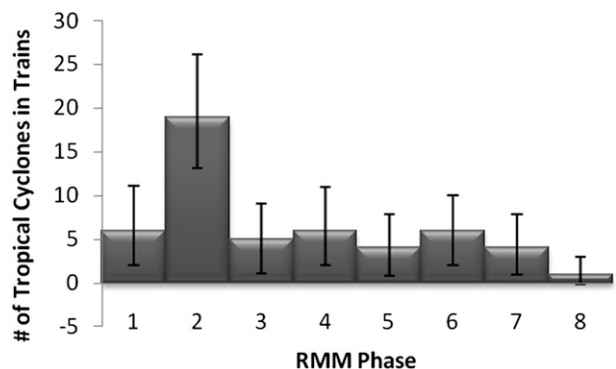


FIG. 11. Total number of tropical cyclones formed in a tropical cyclone train for each RMM phase. Error bars indicate the 95% confidence interval.

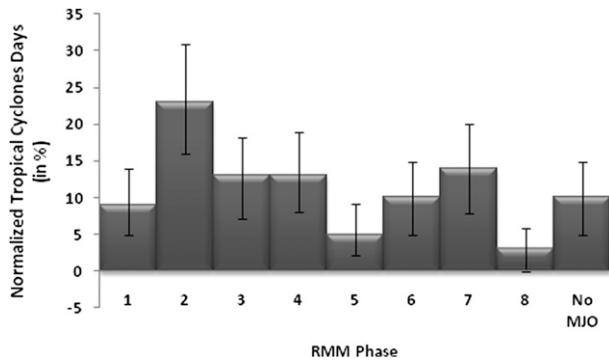


FIG. 12. The distribution of normalized tropical cyclone days for each RMM phase, including a category for normalized tropical cyclone train days when there was no MJO signal. Error bars indicate the 90% confidence interval.

frequently expressed in such conditions. However, what is unique about RMM phase 2 when compared to all other RMM phases is the eastward extension of the AEJ. We hypothesize that this eastward extension allows for AEWs to grow along the AEJ for a larger distance and length of time, which could strengthen AEWs before they leave the coast of West Africa. Also, the downstream half of the AEJ is farthest poleward when compared to all other RMM phases, which adds additional relative vorticity equatorward of this feature over the MDR. Therefore during this period, the AEJ is more capable of generating and maintaining stronger AEWs, which would impact the downstream tropical cyclogenesis over the MDR.

One example of a recent tropical cyclone train occurred during the onset of the Atlantic hurricane season of 2009. Figure 13 is a bar graph showing the RMM amplitude during the 2009 Atlantic hurricane season. Boxes were subjectively placed over the dates when the

MJO amplitude was greater than  $1\sigma$ , highlighting the convectively active or suppressed RMM phases over tropical Africa. Tropical cyclone symbols were placed to mark the date when an Atlantic tropical depression formed according to the National Hurricane Center.

On 3 August, a strong MJO event (amplitude greater than  $2\sigma$ ) entered the Western Hemisphere (phase 8). Six days later on 9 August, the convective signal of the MJO transitioned over the equatorial Indian Ocean (phase 1). Our results suggest that AEW activity increases through convective and environmental modulations over Africa during phase 1. Further, the large-scale conditions over the MDR become more favorable for tropical cyclogenesis to occur. With the RMM indices reading phase 1, the first tropical cyclone of the season, Tropical Storm Anna formed over the eastern tropical Atlantic on 11 August. Anna was followed by Hurricane Bill on 15 August and Tropical Storm Claudette on 16 August.

The MJO signal weakened during RMM phase 2 toward the end of August and began to reintensify during early September reaching RMM phase 4. Only 3 tropical cyclones formed during that September (with only 1 hurricane), which is below the 1974–2009 climatological average of 3.9 September tropical cyclogenesis events and much below the past decade’s (2000–09) hefty average of 5.7 September tropical cyclogenesis events. This anomalously inactive period was a result of unfavorable conditions over the tropical Atlantic as the RMM indices read phases 4 and 5. Note that during early September, the RMM phase space goes backward, from phase 4 to 3. This clockwise rotation of the RMM phase space suggests the strongest background convective signal was associated with a convectively coupled ERW and not the MJO. This will be discussed later as a caveat with the RMM indices.

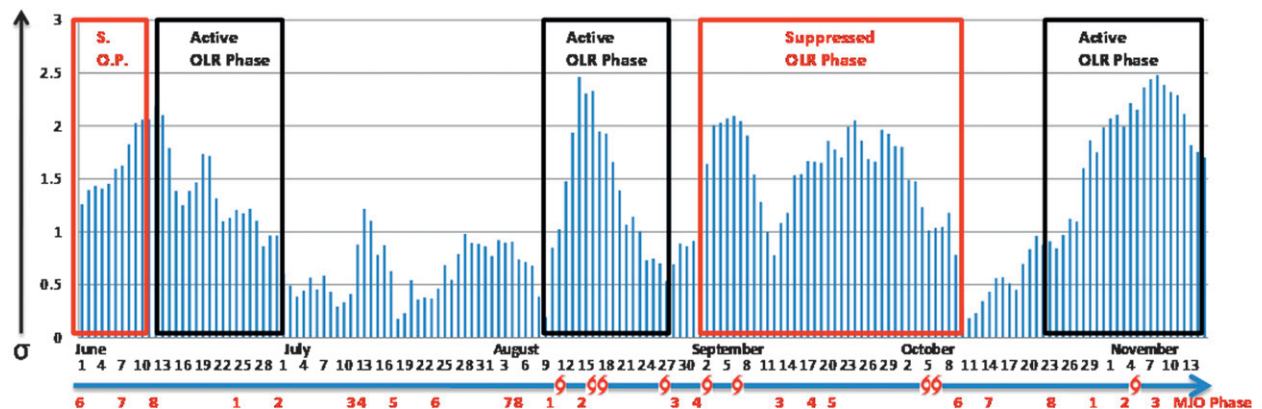


FIG. 13. The 2009 Atlantic hurricane season, highlighting the locally convectively active and suppressed RMM phases, including dates of Atlantic tropical cyclogenesis (at least tropical storm strength). The bar graph represents the amplitude (in  $\sigma$ ) of the Wheeler and Hendon RMM indices. The RMM phases are shown along the bottom line. Note that a tropical cyclone train occurs during mid-August.

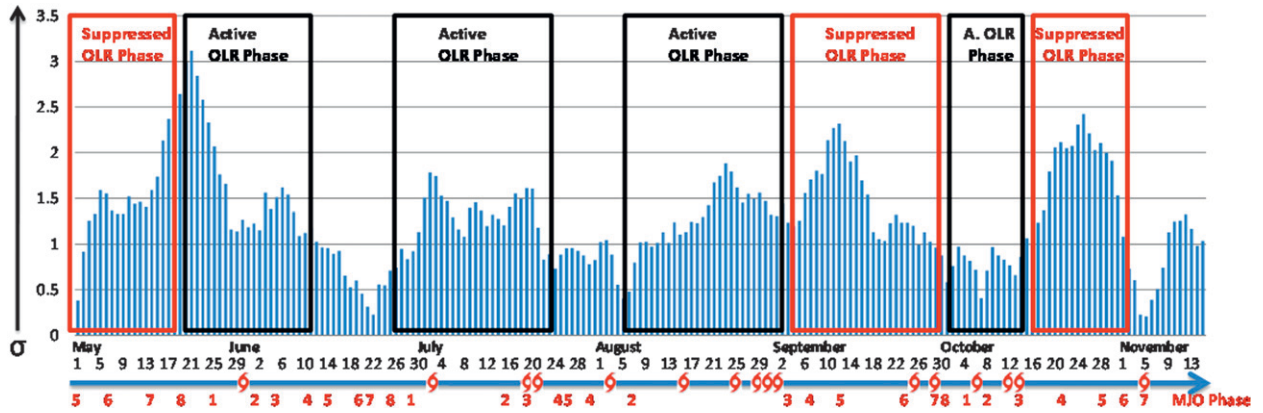


FIG. 14. As in Fig. 14, but for the 2008 Atlantic hurricane season. Note that a tropical cyclone train is observed during the end of August.

A similar train of developing tropical cyclones developed in association with a strong MJO event (amplitude greater than  $1.5\sigma$ ) during late August 2008 (Fig. 14). The MJO amplitude began to increase in early August in a favorable RMM phase 2. The train of developing tropical cyclones occurred after the amplitude peaked at  $1.88\sigma$  on 23 August. Two days later, the first tropical cyclone (Hurricane Gustav) formed on 25 August, followed by Hurricane Hanna on 28 August, Hurricane Ike on 1 September, and Tropical Storm Josephine on 2 September. This period of enhanced tropical cyclone activity ended abruptly during early September as the MJO transitioned into RMM phase 4. The MJO signal remained at fairly high amplitudes in the unfavorable RMM phases (4 and 5) for the majority of September and was associated with no tropical cyclone activity. However, once the MJO signal weakened to less than  $1\sigma$  during late September, a new burst of tropical cyclone activity followed.

We relate these trains of tropical cyclones occurring over the tropical Atlantic when active convection associated with the MJO first begins to propagate northward over southern India and eastward over the equatorial Indian Ocean, taking the shape of an arc (RMM phase 2). We do not rule out interactions between other equatorial wave modes such as convectively coupled atmospheric Kelvin waves, ERWs, and AEWs constructively interfering to produce these periods of enhanced tropical cyclone activity when the RMM amplitude is less than  $1\sigma$ . However, we have higher confidence that these trains of tropical cyclones do not occur when there is a high-amplitude MJO event in an unfavorable RMM phase for tropical cyclone activity over the Atlantic. There are many years when there are no tropical cyclone trains, independent of the MJO. Therefore, predictability is limited; however, if there is a strong MJO genesis event during the Northern Hemispheric

summer, there exists a greater chance of tropical cyclone train activity.

### 5. Discussion and conclusions

The MJO has been shown to modulate weather variability over tropical Africa and the Atlantic. These modulations occur through convective and dynamical processes associated with the MJO. Our results suggest that the MJO directly influences AEW activity. The MJO influences AEW activity by enhancing or suppressing convection locally over Africa, as well as altering the characteristics of the AEJ. This change in AEW activity, along with MJO-induced modulations of large-scale environmental parameters including vertical wind shear, low-level relative vorticity, and moisture, is consistent with coherent variability in tropical cyclogenesis activity over the MDR.

Figure 15 represents a conceptual schematic of the Wheeler and Hendon RMM phase space separating RMM phases associated with the enhancement of the AEJ, the convectively active RMM phases, RMM phases associated with enhanced AEW activity, and RMM phases associated with enhanced MDR tropical cyclone activity. Convection associated with the MJO develops over tropical Africa during a time when the AEJ core is strongest. Enhanced AEW activity over Africa tends to develop locally after a period of enhanced convection. Enhanced MDR tropical cyclogenesis activity occurs during a time when the AEW activity is high over tropical West Africa.

The convective signal of the MJO over Africa is not as large as the signal over the Indian and Pacific Oceans. Distinct phases of the MJO are associated with either enhanced or suppressed convection over Africa. Convection first becomes active over Africa during RMM phase 8 and becomes most enhanced during RMM

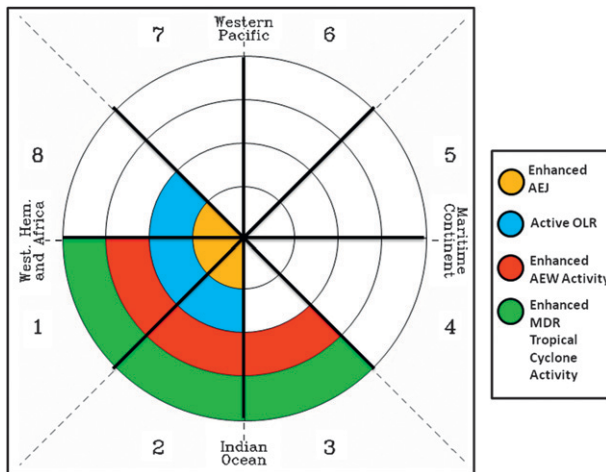


FIG. 15. A schematic RMM phase diagram. The orange shading represents the acceleration of the AEJ, the blue shading represents the convectively active RMM phases over Africa, the red shading represents the RMM phases associated with enhanced AEW activity over Africa, and the green shading represents the RMM phases that are associated with enhanced tropical cyclone activity over the MDR. Note that there are no MJO amplitude implications with this figure.

phases 1 and 2. During RMM phase 3, convection becomes suppressed over tropical Africa, yet is enhanced over the tropical Atlantic. A westward movement of enhanced convection is observed over West Africa during RMM phases 1–3. The following RMM phases 4–7 consist of suppressed convection over sub-Saharan and equatorial Africa.

AEW activity over West Africa is enhanced during RMM phases 1–3. Positive EKE anomalies move westward over Africa and the tropical Atlantic during RMM phases 1–4. The period of anomalously high AEW activity during RMM phase 1, and especially during RMM phase 2, is associated with a more unstable and northward-shifted AEJ. Further, during RMM phase 2 the AEJ extends farther eastward than in any other RMM phase. During RMM phase 4, AEW activity over tropical Africa becomes locally suppressed. These negative EKE anomalies extend westward and amplify during the subsequent RMM phases 5–8. These phases are associated with a southward-shifted AEJ. The AEJ is strongest during RMM phase 8; however it is less unstable due to the influences of the low-level dynamical signal of the MJO.

Consistent with Matthews (2004), Pohl et al. (2009), and Janicot et al. (2010), our results show that ERWs modulate convection (see Fig. 2), along with AEW activity over tropical Africa during the evolution of the MJO. Positive EKE anomalies move westward during RMM phases 1–4 over tropical Africa and the Atlantic,

lagging the westward-propagating convectively active ERW signal by one RMM phase. The strongest negative EKE anomalies move westward during RMM phases 5–8, lagging the westward-propagating convectively suppressed ERW signal by one RMM phase.

We have shown that tropical cyclones develop more frequently during certain RMM phases compared to others (recall Fig. 5). RMM phases 1–3 are favorable phases for tropical cyclone activity over the Atlantic. These results arise due to more favorable atmospheric conditions for tropical cyclone formation, such as reduced vertical wind shear, enhanced moisture, and enhanced low-level cyclonic relative vorticity. Further, these phases are also associated with enhanced AEW activity over tropical Africa, suggestive of more frequent and/or stronger seedlings. Tropical cyclone trains occur most frequently during strong MJO events when convection associated with the MJO first shifts north and eastward over southern India and the northern Indian Ocean (RMM phase 2). RMM phases 7 and 8 are unfavorable for MDR tropical cyclone development. These unfavorable conditions arise from weaker AEW activity over Africa, unfavorable atmospheric conditions for tropical cyclogenesis, and the southward-shifted downstream half of the AEJ.

No perfect indicators of the MJO exist for real-time applications. Occasionally, the Wheeler and Hendon RMM indices do not diagnose a coherent MJO signal even when other indicators suggest it is present. This caveat sometimes arises because Wheeler and Hendon's RMM indices are calculated from data that are averaged from 15°N to 15°S. This latitudinal average may cause problems in exactly positioning the MJO signal along the equator if its convective anomalies are oriented from southeast to northwest from the equator northward. Such patterns can lead to sign swaps along a given longitude line, reducing the expression of its amplitude and occasionally confounding the RMM phase. Further, if the equatorial MJO convective signal interacts with an unfavorable convective phase of another equatorial wave mode, such as an ERW or a Kelvin wave, the RMM assessment of the MJO might be incorrect (Roundy et al. 2009). Further, such interference by equatorial wave modes might cause the RMM principle components to suggest there is an MJO signal when there really is none. For example, the "artificial" MJO signal may be composed of a series of strong equatorial convectively coupled atmospheric Kelvin waves over the equatorial Indian Ocean. Such conditions might result in a fast counterclockwise propagation of RMM indices in phases 1–3 followed by dampening of the RMM amplitude once the active convection associated with the Kelvin waves weaken. Such interference by

ERWs can also yield a clockwise rotation of the RMM indices, suggesting westward propagation (recall Fig. 13).

On the other hand, some such equatorial wave signals might compose part of the anatomy of the MJO. Further work might even indicate that not retaining these different wave modes may allow for a stronger or weaker relationship between Atlantic tropical cyclone activity and the RMM indices. Further, the initiation of the MJO is poorly understood. It is possible that the birth of a new MJO event arises from the interaction between different equatorial wave modes, such as convectively coupled atmospheric Kelvin waves and ERWs. Therefore, by filtering out these wave modes, information relevant to the MJO signal itself might be ignored. This suggests the need for future work to interpret different RMM indices from which the equatorial wave mode signals have been removed, such as those applied by Roundy et al. (2010). We suggest that the relationship between Atlantic tropical cyclone activity and the MJO may change with the removal of the equatorial wave modes.

Accurately positioning a true MJO signal would likely lead to much needed, better quality forecasts on longer time scales for African weather. Better understanding of the association between the MJO and AEWs will help African forecasters to more precisely predict periods of wetness or dryness over Africa on weekly time scales. For instance, Matthews (2004) suggests that the JET2000 field experiment (Thorncroft et al. 2003) failed to observe “strong” AEWs, probably because it was scheduled during an anomalously strong convectively suppressed RMM phase over Africa (phase 5, amplitude greater than  $2\sigma$ ). Our results suggest that if this field experiment had occurred during RMM phases 1–3, rather than RMM phases 5–6, there would have been a higher likelihood to observe strong AEWs over Africa.

Further improved understanding of the association between the MJO and AEW activity might aid forecasters in predicting periods of high or low MDR tropical cyclogenesis activity. Energy companies seek improved intraseasonal predictions of MDR tropical cyclogenesis for commodity trading and protection of their resources. The price of oil is extremely volatile and this volatility increases during periods of anomalously high Atlantic tropical cyclone activity. This volatility arises from the fear of a tropical cyclone tracking into the Gulf of Mexico and interrupting the service provided by oil refineries located there. Our results suggest better skill in predicting periods of enhanced or suppressed tropical cyclone activity over the Atlantic.

*Acknowledgments.* We extend our gratitude to NASA for their Grant NNX09AD08G and to NSF for their Grant 0850642, which supported this research. We are

also grateful to Carl Schreck for his help with data analysis.

## REFERENCES

- Aiyyer, A. R., and C. D. Thorncroft, 2010: Interannual to multi-decadal variability of vertical shear and tropical cyclone activity. *J. Climate*, **24**, 2949–2962.
- Annamalai, H., and J. M. Slingo, 2001: Active/break cycles: Diagnosis of the intraseasonal variability of the Asian summer monsoon. *Climate Dyn.*, **18**, 85–102.
- Frank, W. M., and P. E. Roundy, 2006: The role of tropical waves in tropical cyclogenesis. *Mon. Wea. Rev.*, **134**, 2397–2417.
- Hopsch, S. B., C. D. Thorncroft, K. Hodges, and A. Aiyyer, 2007: West African storm tracks and their relationship to Atlantic tropical cyclones. *J. Climate*, **20**, 2468–2483.
- , —, and K. R. Tyle, 2010: Analysis of African easterly wave structures and their role in influencing tropical cyclogenesis. *Mon. Wea. Rev.*, **138**, 1399–1419.
- Janicot, S., and B. Sultan, 2001: Intraseasonal modulation of convection in the West African monsoon. *Geophys. Res. Lett.*, **28**, 523–526.
- , F. Mounier, N. M. Hall, S. Leroux, B. Sultan, and G. N. Kiladis, 2009: Dynamics of the West African monsoon. Part IV: Analysis of 25–90-day variability of convection and the role of the Indian monsoon. *J. Climate*, **22**, 1541–1565.
- , —, S. Gervois, B. Sultan, and G. N. Kiladis, 2010: The dynamics of the West African monsoon. Part V: The detection and role of the dominant modes of convectively coupled equatorial Rossby waves. *J. Climate*, **23**, 4005–4024.
- Kiladis, G. N., C. D. Thorncroft, and N. M. J. Hall, 2006: Three-dimensional structure and dynamics of African easterly waves. Part I: Observations. *J. Atmos. Sci.*, **63**, 2212–2230.
- , M. C. Wheeler, P. T. Haertel, K. H. Straub, and P. E. Roundy, 2009: Convectively coupled equatorial waves. *Rev. Geophys.*, **47**, RG2003, doi:10.1029/2008RG000266.
- Klotzbach, P. J., 2010: On the Madden–Julian oscillation–Atlantic hurricane relationship. *J. Climate*, **23**, 282–293.
- Knapp, K. R., M. C. Kruk, D. H. Levinson, H. J. Diamond, and C. J. Neumann, 2010: The International Best Track Archive for Climate Stewardship (IBTrACS). *Bull. Amer. Meteor. Soc.*, **91**, 363–376.
- Knutson, T. R., and K. M. Weickmann, 1987: 30–60 day atmospheric circulations: Composite life cycles of convection and circulation anomalies. *Mon. Wea. Rev.*, **115**, 1407–1436.
- , —, and J. E. Kutzbach, 1986: Global-scale intraseasonal oscillations of outgoing longwave radiation and 250-mb zonal wind during Northern Hemisphere summer. *Mon. Wea. Rev.*, **114**, 605–623.
- Landsea, C. W., G. D. Bell, W. M. Gray, and S. B. Goldenberg, 1998: The extremely active 1995 Atlantic hurricane season: Environmental conditions and verification of seasonal forecasts. *Mon. Wea. Rev.*, **126**, 1174–1193.
- Lavender, S. L., and A. J. Matthews, 2009: Response of the West African monsoon to the Madden–Julian oscillation. *J. Climate*, **22**, 4097–4116.
- Leroux, S., and N. M. Hall, 2009: On the relationship between African easterly waves and the African easterly jet. *J. Atmos. Sci.*, **66**, 2303–2316.
- , N. M. J. Hall, and G. N. Kiladis, 2010: A climatological study of transient–mean-flow interactions over West Africa. *Quart. J. Roy. Meteor. Soc.*, **136**, 397–410.

- Liebmann, B., and C. A. Smith, 1996: Description of a complete (interpolated) outgoing longwave radiation dataset. *Bull. Amer. Meteor. Soc.*, **77**, 1275–1277.
- Madden, R. A., and P. R. Julian, 1972: Description of global-scale circulation cells in the Tropics with a 40–50 day period. *J. Atmos. Sci.*, **29**, 1109–1123.
- Maloney, E. D., and D. L. Hartmann, 2000: Modulation of hurricane activity in the Gulf of Mexico by the Madden–Julian oscillation. *Science*, **287**, 2002–2004.
- , and J. Shaman, 2008: Intraseasonal variability of the West African monsoon and Atlantic ITCZ. *J. Climate*, **12**, 2898–2918.
- Matthews, A. J., 2004: Intraseasonal variability over tropical Africa during northern summer. *J. Climate*, **17**, 2427–2440.
- Mekonnen, A., C. D. Thorncroft, and A. R. Aiyer, 2006: Analysis of convection and its association with African easterly waves. *J. Climate*, **19**, 5405–5421.
- Mo, K. C., 2000: The association between intraseasonal oscillations and tropical storms in the Atlantic basin. *Mon. Wea. Rev.*, **128**, 4097–4107.
- Mounier, F., and S. Janicot, 2004: Evidence of two independent modes of convection at intraseasonal timescale in the West African summer monsoon. *Geophys. Res. Lett.*, **31**, L16116, doi:10.1029/2004GL020665.
- , —, and G. N. Kiladis, 2008: The West African monsoon dynamics. Part III: The quasi-biweekly zonal dipole. *J. Climate*, **21**, 1911–1928.
- Murakami, T., L.-X. Chen, A. Xie, and M. L. Shreshta, 1986: Eastward propagation of 30–60-day perturbations as revealed from outgoing longwave radiation data. *J. Atmos. Sci.*, **43**, 961–971.
- Pohl, B., S. Janicot, B. Fontaine, and R. Marteau, 2009: Implication of the Madden–Julian oscillation in the 40-day variability of the West African monsoon. *J. Climate*, **22**, 3769–3785.
- Roundy, P. E., and W. M. Frank, 2004: Applications of a multiple linear regression model to the analysis of relationships between eastward- and westward-moving intraseasonal modes. *J. Atmos. Sci.*, **61**, 3041–3048.
- , C. J. Schreck III, and M. A. Janiga, 2009: Contributions of convectively coupled equatorial Rossby waves and Kelvin waves to the real-time multivariate MJO indices. *Mon. Wea. Rev.*, **137**, 469–478.
- , K. MacRitchie, J. Asuma, and T. Melino, 2010: Modulation of global atmospheric circulation by combined activity in the Madden–Julian oscillation and the El Niño–Southern Oscillation during boreal winter. *J. Climate*, **23**, 3094–3119.
- Simmons, A., S. Uppala, D. Dee, and S. Kobayashi, 2007: ERA-Interim: New ECMWF reanalysis products from 1989 onwards. *ECMWF Newsletter*, No. 110, ECMWF, Reading, United Kingdom, 25–35.
- Sultan, B., S. Janicot, and A. Diedhiou, 2003: The West African monsoon dynamics. Part I: Documentation of intraseasonal variability. *J. Climate*, **16**, 3389–3406.
- Thorncroft, C. D., and M. Blackburn, 1999: Maintenance of the African easterly jet. *Quart. J. Roy. Meteor. Soc.*, **125**, 763–786.
- , and Coauthors, 2003: The JET2000 Project: Aircraft observations of the African easterly jet and African easterly waves. *Bull. Amer. Meteor. Soc.*, **84**, 337–351.
- , N. M. Hall, and G. N. Kiladis, 2008: Three-dimensional structure and dynamics of African easterly waves. Part III: Genesis. *J. Atmos. Sci.*, **65**, 3596–3607.
- Wang, B., and H. Rui, 1990: Dynamics of moist Kelvin–Rossby waves on an equatorial  $\beta$ -plane. *J. Atmos. Sci.*, **47**, 397–413.
- Wheeler, M., and K. M. Weickmann, 2001: Real-time monitoring and prediction of modes of coherent synoptic to intraseasonal tropical variability. *Mon. Wea. Rev.*, **129**, 2677–2694.
- , and H. H. Hendon, 2004: An all-season real-time multivariate MJO index: Development of an index for monitoring and prediction. *Mon. Wea. Rev.*, **132**, 1917–1932.
- Zhang, C., 2005: Madden–Julian oscillation. *Rev. Geophys.*, **43**, RG2003, doi:10.1029/2004RG000158.